Disorder-Induced Localization in Crystalline Pseudo-Binary GeTe–Sb_2Te_3 Alloys between $Ge_3Sb_2Te_6$ and GeTe

Peter Jost, Hanno Volker, Annika Poitz, Christian Poltorak, Peter Zalden, Tobias Schäfer, Felix R. L. Lange, Rüdiger M. Schmidt, Bernd Holländer, Matti R. Wirtssohn, and Matthias Wuttig*

Disorder has a tremendous impact on charge transport in crystalline compounds on the pseudo-binary line between Sb_2Te_3 and GeTe. Directly after crystallization, the pronounced disorder on the cation sublattice renders crystalline $Ge_1Sb_2Te_4$—a composition with a carrier density of the order of 10^{20} cm^{-3}—an Anderson insulator. Annealing, however, induces the reduction of disorder and eventually triggers an insulator-to-metal transition. This study presents data on the electrical properties, the optical conductivity, and structural properties of the pseudo-binary compositions between $Ge_3Sb_2Te_6$ and GeTe. In contrast to the preceding investigations, which rely on the annealing temperature for tuning the electrical properties, this study elucidates the impact of stoichiometry and demonstrates that the stoichiometry may be employed as an alternative control parameter for the metal-to-insulator transition. The combination of annealing temperature and stoichiometry, therefore, provides a rich playground for tailoring disorder and, as a consequence, the transport of charge.

1. Introduction

Phase-change memories exploit the optical or electrical contrast between the amorphous and the crystalline phases of so-called phase-change materials to encode information. Owing to their fast switching properties and pronounced optical contrast, especially thin films of the pseudo-binary $(GeTe)_x$-$(Sb_2Te_3)_{1-x}$ system are employed in rewritable optical data storage.[1–3] In some of these pseudo-binary compounds, the conductivity of the crystalline state is not constant but can be increased by several orders of magnitude on annealing,[4–8] which is important for the development of electrical phase-change memory devices.

Room-temperature sputter-deposition of the pseudo-binary $(GeTe)_x$-$(Sb_2Te_3)_{1-x}$ alloys between $Ge_1Sb_4Te_7$ ($x = 1/3$) and $Ge_3Sb_2Te_6$ ($x = 3/4$) yields amorphous films. On crystallization, these alloys form cubic, rock-salt-like crystal structures,[9] where the anion sublattice is completely filled by tellurium atoms, while the cation sublattice is randomly occupied by germanium and antimony as well as (structural) vacancies. These vacancies result from the cation (Ge, Sb) versus anion (Te) imbalance. In $Ge_1Sb_2Te_4$, for instance, there are four anions, but only three cations per formula unit. As a consequence, one quarter of the cation lattice sites remains empty. On annealing the rock-salt-like GeSbTe compounds between $Ge_1Sb_4Te_7$ and $Ge_3Sb_2Te_6$, the species on the cation sublattice start ordering into layers. Eventually, the metastable rock-salt-like cubic structure transforms into the thermodynamically stable hexagonal structure.[9]

Recently, an in-depth study focusing on $Ge_1Sb_2Te_4$ ($x = 1/2$) revealed that the unusual electrical properties of these GeSbTe compounds and the aforementioned annealing effect in the electrical conductivity are not a mere consequence of this crystallographic cubic-to-hexagonal transition, but originate from disorder-induced localization effects.[6] On crystallization, the occupancy disorder generated by the initially random cation sublattice of the metastable rock-salt like structure (Ge, Sb, and vacancies) gives rise to charge carrier localization and renders $Ge_1Sb_2Te_4$ an Anderson insulator, i.e., the system displays a vanishing zero-temperature conductivity $\sigma(T \rightarrow 0) = 0$. On annealing, the ordering of the cations into layers significantly reduces this disorder. As a consequence, the character of the electron wavefunctions at the Fermi level changes from localized to delocalized states and the system becomes metallic.

We note in passing that the structural disorder also affects the thermal conductivity (transition from glass like to crystal like heat conduction in the crystalline state).[10]

Later, density functional theory (DFT) calculations performed by Zhang et al. on $Ge_1Sb_2Te_4$ verified the formation of localized electronic states. Moreover, these calculations provided first insight into the microscopic origin of the electron

Dr. P. Jost, Dr. H. Volker, A. Poitz, C. Poltorak, Dr. P. Zalden, T. Schäfer, F. R. L. Lange, R. M. Schmidt, M. R. Wirtssohn, Prof. M. Wuttig
I. Institute of Physics (IA)
RWTH Aachen University
Sommerfeldstr. 14, 52074 Aachen, Germany
E-mail: jost@physik.rwth-aachen.de

Dr. B. Holländer
Peter Grünberg Institut (PGI-9)
Forschungszentrum Jülich GmbH
52425 Jülich, Germany

Dr. B. Holländer, Prof. M. Wuttig
JARA-Fundamentals of Future Information Technologies

DOI: 10.1002/adfm.201500848

Table 1. An overview on the properties of the pseudo-binary compounds between Sb_2Te_3 and GeTe. The stoichiometry parameter x refers to $(GeTe)_x$-$(Sb_2Te_3)_{1-x}$. From top to bottom, the structure, the presence of a marked annealing effect in the electrical conductivity, the room-temperature conductivity, the temperature coefficient of the resistivity (sign), and the classification of the $\rho(T)$ behavior with respect to metal–insulator transitions (MIT) are listed (data from the literature).[6,16,35] While the systems in the range x = 1/3 ... 3/4 follow a generic ($Ge_1Sb_2Te_4$-like) behavior, the properties change in the region between $Ge_3Sb_2Te_6$ and GeTe (x = 3/4 ... 1).

	$Ge_1Sb_2Te_4$-like				$Ge_8Sb_2Te_{11}$-like	GeTe-like
	$Ge_1Sb_4Te_7$	$Ge_1Sb_2Te_4$	$Ge_2Sb_2Te_5$	$Ge_3Sb_2Te_6$	$Ge_8Sb_2Te_{11}$	GeTe
x	1/3	1/2	2/3	3/4	8/9	1
Structure	cub/hex	cub/hex	cub/hex	cub/hex	rhomb/cub	rhomb/cub
Annealing effect	Yes	Yes	Yes	Yes	Minor	Negligible
σ (300 K)[S cm^{-1}]	2 ... 2600	3 ... 2200	10 ... 2400	20 ... 1700	≈120	1800 ... 2300
sgn ($d\rho/dT$)	−/+	−/+	−/+	−/+	≈0	+
Behavior	MIT	MIT	MIT	MIT	?	Metallic

localization in the GeSbTe compounds: The formation of localized states at the Fermi level is directly linked to the presence of vacancy clusters.[11] This result implies that the disorder in the distribution of germanium and antimony atoms on the cation sublattice in rock-salt like $Ge_1Sb_2Te_4$ has a negligible impact on the nature of the wave functions, whereas the spatial distribution of vacancies is crucial. In line with the already existing understanding of the relaxation processes, the calculations indicate that the ordering of vacancies into layers is energetically favorable (50 meV per atom). However, as the removal of the germanium versus antimony disorder is associated with an almost negligible energy gain (5 meV per atom), it is questionable if the germanium versus antimony disorder can really be eliminated on annealing.

Breznay et al.[12] have performed an in-depth study of the quantum corrections to the conductivity on the metallic side of the metal–insulator transition in $Ge_1Sb_2Te_4$ and the recent findings of Nukala et al.[13] stress the relevance of disorder-induced metal–insulator transitions even in single-crystalline GeTe nanowire devices. Volker et al.[8] revisited the metal–insulator transition in $Ge_1Sb_2Te_4$ in the true zero-Kelvin limit. Their low-temperature measurements down to 0.35 K allow identifying the transition point and demonstrate that the system is suitable to study fundamental questions on disorder-driven metal–insulator transitions.

Table 1 presents a summary of the properties of the most common compositions in the $(GeTe)_x$-$(Sb_2Te_3)_{1-x}$ system. While the compounds between $Ge_1Sb_4Te_7$ and $Ge_3Sb_2Te_6$ display the aforementioned irreversible cubic-to-hexagonal transition on heating,[9] $Ge_8Sb_2Te_{11}$ and GeTe show a reversible structural transition from a rhombohedrally distorted low-temperature phase to a cubic high-temperature phase.[14,15]

As was already pointed out by Siegrist et al.,[6] the compositions in the range between $Ge_1Sb_2Te_4$ and $Ge_3Sb_2Te_6$ follow a generic ($Ge_1Sb_2Te_4$-like) behavior: In all these compositions, the conductivity of the crystalline state increases by at least two orders of magnitude on annealing while the temperature coefficient of the resistivity changes from non-metallic ($d\rho/dT < 0$) to metallic ($d\rho/dT > 0$) behavior. GeTe, by contrast, lacks a comparable annealing effect and $Ge_8Sb_2Te_{11}$—a material which was recently shown to display favorable thermoelectric properties[16]—exhibits a conductivity close to the minimum metallic conductivity. Hence, the electrical characteristics change markedly in the region between $Ge_3Sb_2Te_6$ and GeTe. Against this background, a thorough investigation focusing on the alloys between $Ge_3Sb_2Te_6$ and GeTe appears worthwhile.

To this end, we prepared eight stoichiometries between $Ge_3Sb_2Te_6$ and GeTe by cosputtering from stoichiometric $Ge_3Sb_2Te_6$, $Ge_8Sb_2Te_{11}$, and GeTe targets. Following the experimental procedures already applied and outlined in a previous study,[6] we characterized the electrical, optical, and structural properties of the films by sheet resistance, Hall effect, Fourier transform infrared spectroscopy (FT-IR), and X-ray diffraction (XRD). However, in contrast to preceding investigations,[4–7] where the annealing temperature T_a was varied at constant stoichiometry x (Siegrist et al.:[6] T_a = 150 ... 325 °C, x = 1/2), we varied the stoichiometry rather than the annealing temperature (T_a = 250/275 °C, x = 3/4 ... 1).

2. Experimental Section

All samples were produced by magnetron sputtering from 10 cm cathodes in a Von Ardenne LS 320S sputter system. The sputter chamber was pumped down to background pressures of 2×10^{-6} mbar or better prior to deposition. During the depositions, an argon flow of 20 sccm yielded process pressures in the 10^{-3} mbar range. The samples were installed on a rotating sample holder, which facilitates the simultaneous deposition on multiple substrates. The films of $Ge_3Sb_2Te_6$, $Ge_8Sb_2Te_{11}$, and GeTe were created by DC sputtering from stoichiometric targets of the three compositions. In addition, three stoichiometries in the range between $Ge_3Sb_2Te_6$ and $Ge_8Sb_2Te_{11}$ as well as two compositions in the range between $Ge_8Sb_2Te_{11}$ and GeTe were produced by cosputtering from either the $Ge_3Sb_2Te_6$ and the $Ge_8Sb_2Te_{11}$ targets or the $Ge_8Sb_2Te_{11}$ and the GeTe targets.

For each stoichiometry, two independent sputter runs were carried out to produce thin films (≈80 nm) and thick films (400–600 nm). The thin films were sealed by RF sputtering a capping layer of about 80 nm from a $(ZnS)_{80}(SiO_2)_{20}$ target. Glass slides (cover glasses for microscopy), single side polished (SSP) (100) silicon pieces, and double side polished (DSP) (100) silicon pieces were used as substrates. For all electrical

Table 2. Characterization techniques and corresponding substrates. Thick/thin refers to whether the thickness of the GeSbTe layer was ≈80 nm or 400–600 nm.

Technique	Substrate	Film thickness
X-ray diffraction	Glass (20 mm × 20 mm)	Thick
ρ and n_{hall}	Glass (10 mm × 10 mm)	Thin
$\rho(T)$ on cryst.	Glass (20 mm × 20 mm)	Thin
Optical properties	Glass, silicon (100) SSP, silicon (100) DSP (all in 20 mm × 20 mm)	Thick

measurements, a van der Pauw contact geometry was used, where first the metal contacts (10 nm Cr + 80 nm Au) and subsequently the GeSbTe+$(ZnS)_{80}(SiO_2)_{20}$ films were deposited through shadow masks. **Table 2** gives an overview on the characterization techniques and the corresponding substrates.

All GeSbTe films were amorphous as-deposited. The crystallization and annealing were performed under argon atmosphere in a tube furnace, which allows to probe the film's sheet resistance during heating.

XRD measurements in grazing incident geometry (angle of incidence $\omega = 1°$) were performed by a Philips X'Pert pro system (copper K_α radiation).

The low-temperature electrical measurements (resistivity down to 2 K and Hall effect) were carried out in a Quantum Design Physical Properties Measurement System (PPMS).

Optical spectra in the range between 0.05 and 1 eV were recorded by a Bruker IFS 66 v/S IR-spectrometer. For each stoichiometry, the following reflectance (R) and transmittance (T) spectra were recorded on the various substrates: Glass (only >0.5 eV, R&T), Si SSP (R), and Si DSP (R&T). The data analysis followed the procedure already proposed by Shportko et al.[17] A parameterized dielectric function model consisting of a dielectric background, a Tauc–Lorentz oscillator,[18] and a Drude model (free carrier absorption)[19] was adjusted to reproduce the 5 reflectance and transmittance spectra simultaneously. This fit process was carried out using the SCOUT software package.[20] The Drude model is given by

$$\chi_{\text{Drude}}(\omega) = -\frac{\omega_p^2}{\omega^2 + i\omega\Gamma} \tag{1}$$

where plasma frequency $\omega_p^2 = \frac{e^2 n}{\varepsilon_0 m^*}$ and damping $\Gamma = \tau^{-1}$ can be employed to determine the ratio of carrier density to effective mass $\frac{n}{m^*}$, the carrier relaxation time τ, and the DC extrapolation of the optical conductivity in terms of the Drude model $\sigma_{\text{opt}} := \sigma_{\text{opt}}(\omega = 0) = \varepsilon_0 \omega_p^2 \tau$.

The stoichiometry was verified by Rutherford backscattering (RBS) and energy-dispersive X-ray spectroscopy (EDX) measurements. The RBS experiments were performed at the 1.7 MV Tandem Accelerator at Forschungszentrum-Jülich. A beam of He^+ ions with an energy of 1.4 MeV was used to irradiate the samples with a fixed ion dose of 15 µC. The detector counting the backscattered ions was positioned at an angle of 170°. The RUMP software[21] was used to analyze the spectra.

The EDX data were obtained by a FEI Helios 650 NanoLab system. The electron beam (10 keV and 0.4 nA) scanned a 200 µm × 300 µm-sized area. The setup was calibrated by measuring a Cu sample at the same beam parameters. The AZtec 2.1 software was used for recording and analyzing the data.

3. Results and Discussion

3.1. Stoichiometry

We determined the stoichiometry of the films by the following independent methods:

1) From the nominal compositions of the sputter targets and the deposition rates;
2) Rutherford backscattering (RBS);
3) Energy-dispersive X-ray spectroscopy (EDX).

For the sake of brevity, we refer to the Supporting Information for a detailed comparison of the three methods. As can be seen in the Supporting Information, both, RBS and EDX, indicate a minor germanium excess, which results from the sputter process. Besides this insignificant deviation from the nominal composition, the deposition-rate-based estimates are perfectly in line with the RBS and EDX results, a clear confirmation of the effectiveness of the cosputter process.

As the three methods are in good agreement, we will simply refer to the stoichiometries obtained from the deposition rates in the following discussion. The corresponding germanium, antimony, and tellurium concentrations as well as the parameterization "x" along the pseudo-binary tie line

$$(GeTe)_x + (Sb_2Te_3)_{1-x} \tag{2}$$

are summarized in **Table 3**.

3.2. Crystallization and Annealing Effect

It has already been demonstrated[6,22–24] that heating experiments such as those presented in **Figure 1** can readily characterize the crystallization and annealing behavior of phase-change alloys: Starting with an initially as-deposited

Table 3. The table lists the stoichiometries of the compositions investigated in this work. x refers to the parameterization given by Equation (2). The results obtained from the sputter-target compositions and the deposition rates are presented. See the Supporting Information for the RBS and EDX results.

	x	Ge	Sb	Te
$Ge_3Sb_2Te_6$	0.750	0.273	0.182	0.545
	0.808	0.313	0.149	0.537
	0.825	0.327	0.138	0.535
	0.847	0.344	0.124	0.531
$Ge_8Sb_2Te_{11}$	0.889	0.381	0.095	0.524
	0.932	0.423	0.062	0.515
	0.946	0.438	0.050	0.512
GeTe	1.000	0.500	0.000	0.500

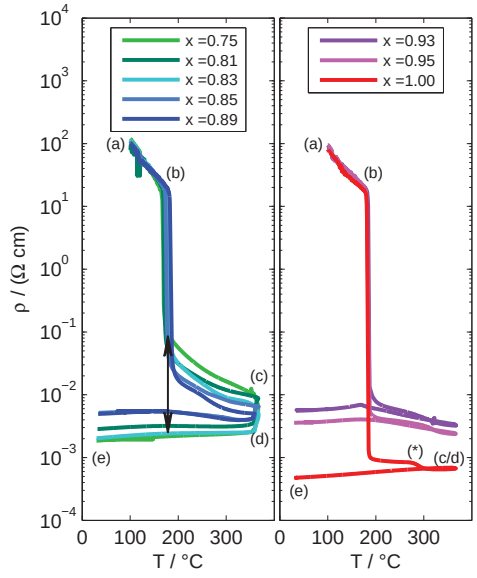

Figure 1. The resistivity of initially as-deposited amorphous films on heating and subsequent cooling. The color code x refers to the stoichiometry of the film. a) Start in the highly resistive amorphous phase. b) Crystallization. c,d) Waiting at 350 °C for 30 min. d,e) Cooling down to room temperature. (*) crystallization of segregated germanium in GeTe ($x = 1$). The black arrow highlights the annealing effect.

amorphous film at room temperature, the sheet resistance of the film is monitored while the film is heated and subsequently cooled. The data depicted in Figure 1 were recorded using the following thermal treatment:

1) Heating up to 350 °C (5 K min^{-1});
2) Annealing at 350 °C for 30 min;
3) Cooling down to room temperature.

The interpretation of the $\rho(T)$ curves can be illustrated by the examples of the two endpoints of our stoichiometric range, i.e., $Ge_3Sb_2Te_6$ and GeTe ($x = 0.75$ and $x = 1.00$). At the beginning, the films are in the as-deposited amorphous phase and, therefore, display large resistivities, which decrease on heating (Arrhenius-like temperature dependence of the conductivity). When the crystallization temperatures are reached ($Ge_3Sb_2Te_6$: 170 °C, GeTe: 185 °C), the resistivities sharply drop by several orders of magnitude ($Ge_3Sb_2Te_6$: 10^2, GeTe: 10^4); a clear consequence of the electrical contrast of phase-change materials.

From this point on, the films are fully crystalline. On further annealing, the resistivity of the crystalline $Ge_3Sb_2Te_6$ film reduces again by almost two orders of magnitude. The fact that the data points recorded on heating do not coincide with those recorded on cooling clearly indicates that the reduction in resistivity is an irreversible effect. As has been demonstrated by Siegrist et al. by the example of $Ge_1Sb_2Te_4$,[6] this annealing effect in the electrical resistivity of the crystalline state is concomitant with an insulator to metal transition.

By contrast, further heating has almost no effect on the electrical resistivity of the crystalline GeTe film. Hence, for this composition, a comparable annealing effect is absent. As is discussed in the Supporting Information to a previous study[6] the minor step above 250 °C (see (*)) can be attributed to the crystallization of segregated amorphous excess-germanium.

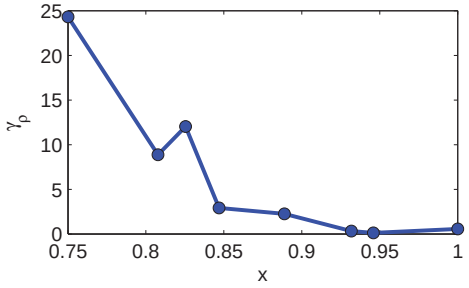

Figure 2. Magnitude of the annealing effect as defined by Equation (3) as function of stoichiometry x. On going from $Ge_3Sb_2Te_6$ ($x = 0.75$) toward GeTe ($x = 1$), the annealing effect vanishes in the vicinity of $Ge_8Sb_2Te_{11}$ ($x = 8/9$).

On examining the entire stoichiometric range between $Ge_3Sb_2Te_6$ and GeTe, two observations become evident: First, there seems to be a slight increase in the crystallization temperature on going from $Ge_3Sb_2Te_6$ to GeTe (170 °C → 185 °C). This finding is not surprising as it fits in the overall picture of the crystallization temperature increasing monotonically from Sb_2Te_3 to GeTe.[1]

Second, the annealing effect is very prominent on the Sb_2Te_3 side (low x), whereas it disappears toward GeTe ($x = 1$). This becomes even more evident from **Figure 2**, where the parameter γ_ρ is plotted, which measures the magnitude of the annealing effect by comparing the resistivities obtained on heating to those recorded on cooling, measured at 200 °C

$$\gamma_\rho := \left.\frac{\rho^{\text{heating}}}{\rho^{\text{cooling}}}\right|_{T=200\,^\circ C} - 1 \tag{3}$$

With increasing GeTe content, the annealing effect gradually fades out and disappears in the vicinity of $Ge_8Sb_2Te_{11}$ ($x = 8/9$).

At this point, the analysis can focus either on the impact of annealing temperature T_a or on the impact of stoichiometry x. As Zhang et al.,[4] Prokhorov et al.,[5] Siegrist et al.,[6] and Volker et al.[8] have already done the former and elucidated the impact of annealing temperature on step-annealed films of $Ge_1Sb_2Te_4$, elaborating the stoichiometry aspect seems most rewarding. For this reason, the data that will be discussed in the following were obtained from initially as-deposited amorphous films, which were annealed (and crystallized) at 275 °C (GeTe) and 250 °C (all other compositions) prior to the measurements, i.e., we varied the stoichiometry x, but kept the annealing temperature constant (275/250 °C).

For GeTe, the larger annealing temperature of 275 °C was chosen because of the aforementioned crystallization of segregated amorphous germanium in sputtered GeTe. Siegrist et al.[6] observed this crystallization on annealing at 250 °C. Thus, following exactly their heating procedure, but increasing the annealing temperature to 275 °C ensures the absence of amorphous germanium in the films. At a first glance, the statement that the germanium crystallization occurs on annealing at 250 °C appears to conflict with the data presented in Figure 1, where the step-like decrease in resistivity

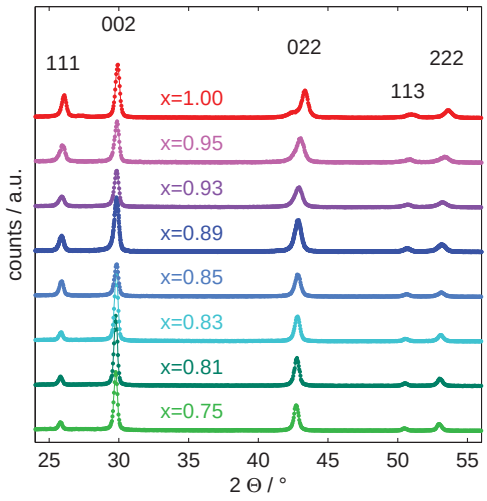

Figure 3. XRD scans performed in grazing-incidence geometry. The colorcode refers to the stoichiometry *x*. No signs of amorphous residues are discernible. All films display rhombohedral peak patterns. The tiny hump visible in the pattern recorded on the GeTe film ($x = 1$) at 27.3° can be attributed to minor inclusions of crystalline germanium. The Miller indices labeling the peaks refer to the cubic basis-system.

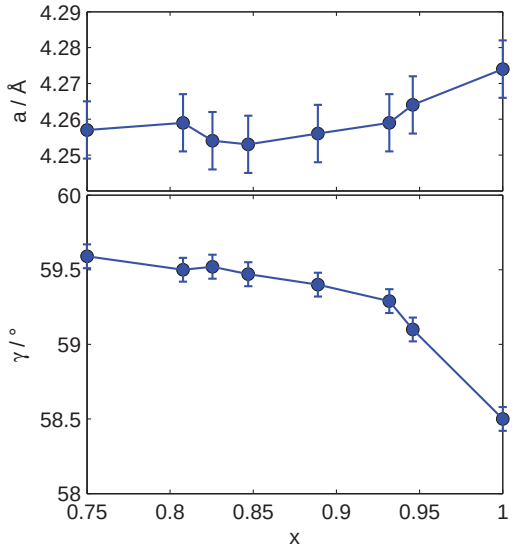

Figure 4. The lattice parameter *a* and the rhombohedral angle γ as derived from the XRD scans depicted in Figure 3. While the lattice parameter a remains constant within the margin of error, the rhombohedral angle gradually decreases toward GeTe ($x = 1$).

attributed to this effect appears at approximately 275 °C. This perceived discrepancy is also discussed in the Supporting Information.

3.3. Structural Properties

Figure 3 presents the XRD scans performed in grazing-incidence geometry on the films annealed at 250/275 °C. As expected, the absence of a diffuse background indicates that there are no amorphous residues in the films.

It is well established that GeTe forms a rhombohedrally distorted rock-salt-like structure at room temperature, where the cation sublattice is occupied by germanium and the anion sublattice is occupied by tellurium.[9,14,15] As was already mentioned, the meta-stable cubic structures of the GeSbTe compounds between $Ge_1Sb_4Te_7$ and $Ge_3Sb_2Te_6$ may be regarded as cubic modifications of the rhombohedral GeTe structure, where the cation sublattices are filled by germanium, antimony, and vacancies.[2,9,25]

Against this background, it is not surprising, that the peak patterns in Figure 3 fit to rhombohedral unit cells. The tiny hump which appears in the measurement of GeTe at 27.3° results from minor inclusions of crystalline germanium, a consequence of the aforementioned germanium segregation in this particular composition.

Assuming a rhombohedral unit cell, the lattice parameter *a* and the rhombohedral angle γ can be deduced from the positions of the Bragg reflections. Both parameters are plotted as a function of stoichiometry in **Figure 4**. Apparently, the lattice constant remains almost unchanged within the margin of error, while the rhombohedral angle follows a clear trend: Starting from a nearly cubic structure ($\gamma \approx 60°$) at $Ge_3Sb_2Te_6$ ($x = 0.75$), the rhombohedral angle gradually decreases toward GeTe. It is noteworthy that both lattice parameters (*a* and γ) display only smooth and gradual variations and that no abrupt structural transitions – such as the cubic-hexagonal transition in the $Ge_1Sb_2Te_4$ system – are discernible on varying the stoichiometry between $Ge_3Sb_2Te_6$ and GeTe.

3.4. Electrical Properties

The following discussions will reveal striking analogies to the behavior of the electrical transport parameters observed on increasing the annealing temperature of the $Ge_1Sb_2Te_4$-like compositions (see Table 1). It is, therefore, instructive to briefly review the situation in $Ge_1Sb_2Te_4$. To this end, **Figure 5** depicts the electrical transport parameters of $Ge_1Sb_2Te_4$ ($x = 1/2$) as functions of annealing temperature (data from Siegrist et al.).[6]

Hall effect and thermopower measurements agree that crystalline GeSbTe films are p type.[4–7,16,26,27] Moreover, there is little doubt that $Ge_1Sb_2Te_4$ films which have been annealed at temperatures above 250 °C can be regarded as ordinary degenerate semiconductors, where the Fermi level intersects the valence band and the wave functions in the vicinity of the Fermi level are extended Bloch waves.[6]

Bahl and Chopra[28] pointed out that the electrical properties of crystalline (rhombohedral) GeTe can be readily understood by a simple model consisting of a parabolic and isotropic valence band maximum. By analogy with other IV–VI alloys, they assumed the relevant valence band maximum to be situated at the L point leading to a fourfold valley degeneracy ($M = 4$). By adopting their considerations to $Ge_1Sb_2Te_4$, Siegrist et al.[6] conducted an analysis of the transport properties of the step-annealed $Ge_1Sb_2Te_4$ films within the same framework. This analysis confirmed that the properties of the $Ge_1Sb_2Te_4$

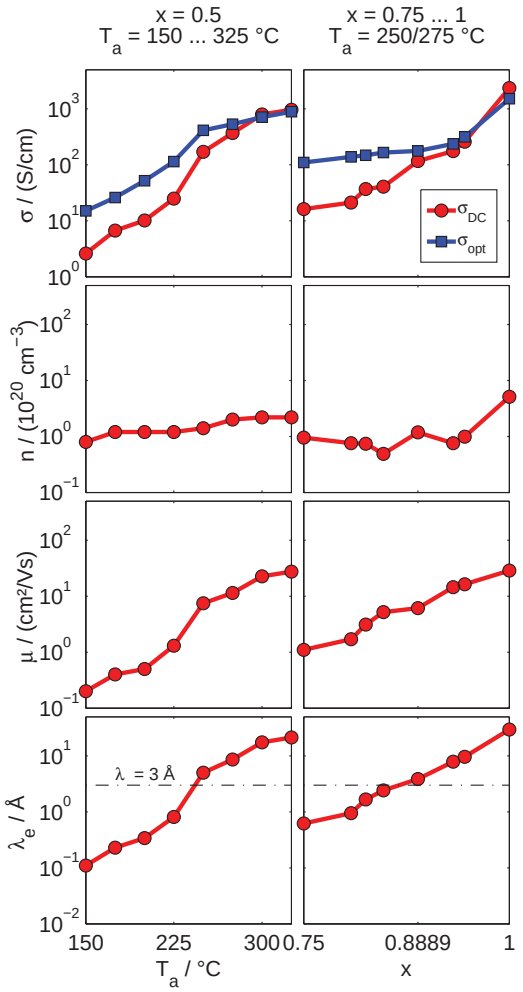

Figure 5. From top to bottom, the DC and optical conductivities, the Hall carrier densities, the Hall mobilities, and the electron mean free paths are shown. While the left-hand side (taken from the literature)[6] depicts the data recorded on increasing the annealing temperature T_a of $Ge_1Sb_2Te_4$ ($x = 1/2$), the right-hand side (this work) presents the corresponding data obtained on sweeping the stoichiometry x at constant T_a. Apparently, increasing T_a of $Ge_1Sb_2Te_4$ and increasing x in $(GeTe)_x$-$(Sb_2Te_3)_{1-x}$ induce the same changes in the electrical properties.

films annealed at high temperatures (≳250 °C) may very well be explained in terms of a degenerate semiconductor with extended Bloch states at the Fermi level.

By contrast, crystalline $Ge_1Sb_2Te_4$ films annealed at temperatures below 200 °C display transport parameters, which clearly conflict with the assumption of Bloch states at the Fermi level. As can be seen from the second column in **Table 4** and from the left-hand side of Figure 5, the Bloch state model yields unreasonable parameters for the 150 °C annealed film.

For instance, the carrier mobility assumes values reminiscent of amorphous semiconductors and the mean free path is much smaller than the interatomic spacing ($a \approx 3$ Å), a clear violation of the Ioffe–Regel criterion.[29,30] As Siegrist et al.[6] have already argued, the breakdown of charge transport via Bloch states at low annealing temperatures can be attributed to localization effects resulting from the disorder on the cation sublattice of the meta-stable rock-salt-like structure.

The right-hand sides in Figure 5 and Table 4 present the corresponding transport parameters of the cosputtered stoichiometries in the $(GeTe)_x$-$(Sb_2Te_3)_{1-x}$ system. Apparently, increasing the GeTe content in the $(GeTe)_x$-$(Sb_2Te_3)_{1-x}$ system evokes the same changes in the charge transport parameters as an increase of the annealing temperature of $Ge_1Sb_2Te_4$ (plots on the left-hand side). In particular, the following parallels are discernible:

1) The DC conductivity can be enhanced by more than two orders of magnitude.
2) The enhancement in the DC conductivity is concomitant with an increase in the optical conductivity σ_{opt}. However, the latter clearly exceeds the DC conductivity σ_{DC} first, but then coincides with σ_{DC} at high annealing temperatures/large GeTe contents.
3) The Hall carrier density n remains almost constant. Consequently, the increase in conductivity stems almost exclusively from a mobility increase.
4) The analysis in terms of Bloch states at the Fermi level yields reasonable parameters at high annealing temperatures/large GeTe contents, but in both systems the failure of this model at low annealing temperatures/small x becomes evident from the unrealistically short mean free path falling below the interatomic spacing of 3 Å.

These striking parallels immediately raise the question, whether the analogy between both systems also persists in the low-temperature domain, i.e., does the $(GeTe)_x$-$(Sb_2Te_3)_{1-x}$ system also undergo a metal–insulator transition?

The resistivities of the cosputtered films as a function of measurement temperature are depicted in **Figure 6**. The overall behavior is reminiscent of the behavior seen by Siegrist et al.[6] and Volker et al.[8] The question whether the films are metallic or insulating, i.e., whether the zero-temperature conductivity is finite ($\sigma(0\ K) > 0$) or vanishing ($\sigma(0\ K) = 0$), can only be answered by proper low-temperature extrapolations.

In the critical region, i.e., close to the metal-to-insulator transition point, the conductivity typically obeys the following behavior, where $\sigma_0 > 0$ and $\sigma_0 < 0$ indicate metallic/insulating samples[31–34]

$$\sigma(T) = \sigma_0 + \beta\sqrt{T} \tag{4}$$

As can be seen from **Figure 7**, the extrapolation according to Equation (4) is successful in the displayed range between $x = 0.75$ and $x = 0.85$. As the films with $x \geq 0.83$ display $\sigma_0 > 0$, they are clearly metallic. By contrast, the $x \leq 0.81$ films must be insulators. Hence, we observe an insulator-to-metal transition on increasing the GeTe-content from $x = 0.81$ to $x = 0.83$.

In summary, the stoichiometry variation between $Ge_3Sb_2Te_6$ and GeTe at constant annealing temperature ($x = 0.75$ ... 1.00, $T_a = 250/275$ °C) induces the same behavior as increasing the annealing temperature of $Ge_1Sb_2Te_4$ at constant stoichiometry ($x = 1/2$, $T_a = 150$. 325 °C).

Table 4. The two columns on the left-hand side present the transport parameters of the annealing series on $Ge_1Sb_2Te_4$ (from Siegrist et al.)[6] whereas the eight columns on the right-hand side reflect the corresponding parameters obtained in the course of this work on varying the stoichiometry x in the $(GeTe)_x$–$(Sb_2Te_3)_{1-x}$ system. From top to bottom, the following parameters are listed: The stoichiometry, the annealing temperature, the DC conductivity, the optical conductivity, the Hall carrier density, the ratio of carrier density to effective mass from the FT-IR Drude part, the Hall mobility, the carrier relaxation time, the effective mass, the Fermi radius, the Fermi level, and the electron mean free path. See the Supporting Information of the referenced study[6] for details on the calculations of m^*, k_F, E_F, and λ_e. In some cases, where the analysis of the optical spectra does not allow determining the two Drude parameters $\omega_p^2 \propto n/m^*$ and τ independently, only upper and lower limits can be derived for τ and n/m^*. This problem is also discussed by Siegrist et al.[6]

	$Ge_1Sb_2Te_4$		$(GeTe)_x$–$(Sb_2Te_3)_{1-x}$							
x	0.50	0.50	0.75	0.81	0.83	0.85	0.89	0.93	0.95	1.00
T_a [°C]	150	325	250	250	250	250	250	250	250	275
σ_{DC} [S cm^{-1}]	2.6	962	16	21	37	41	117	176	258	2360
σ_{opt} [S cm^{-1}]	15	885	110	139	148	165	177	237	315	1520
n [10^{20} cm^{-3}]	0.8	2.2	1.0	0.8	0.7	0.5	1.2	0.8	1.0	5.1
$n\frac{m_e}{m^*}$ [10^{20} cm^{-3}]	$\gtrsim$0.5	5.8	$\gtrsim$3.6	$\gtrsim$7.0	$\gtrsim$8.8	$\gtrsim$9.8	≈6.5	6.8	5.7	21.3
μ [cm^2 V^{-1} s^{-1}]	0.2	27.5	1.1	1.7	3.1	5.2	6.1	14.5	16.3	28.8
τ [fs]	$\lesssim$1.0	5.5	$\lesssim$1.1	$\lesssim$0.7	$\lesssim$0.6	$\lesssim$0.6	≈1.0	1.2	2.0	2.5
m^*/m_e	$\lesssim$1.5	0.4	$\lesssim$0.3	$\lesssim$0.1	$\lesssim$0.1	$\lesssim$0.1	≈0.2	0.1	0.2	0.2
k_F [10^7 cm^{-1}]	0.83	1.17	0.89	0.82	0.82	0.71	0.96	0.82	0.90	1.56
E_F [eV]	$\gtrsim$0.02	0.14	$\gtrsim$0.11	$\gtrsim$0.24	$\gtrsim$0.30	$\gtrsim$0.39	≈0.19	0.23	0.18	0.39
λ_e [Å]	0.11	21.3	0.62	0.95	1.67	2.42	3.9	7.9	9.7	29.6

4. Conclusions

Starting from the annealing effect[4,5,7,22] and the metal–insulator transition,[6,8] which have been observed in the $(GeTe)_x$-$(Sb_2Te_3)_{1-x}$ systems between $Ge_1Sb_4Te_7$ and $Ge_3Sb_2Te_6$, we have analyzed the structural and electrical properties as well as the optical conductivity of crystalline $(GeTe)_x$-$(Sb_2Te_3)_{1-x}$ films between $Ge_3Sb_2Te_6$ and GeTe.

It turns out that the annealing effect in the electrical conductivity of the crystalline state, which is still very prominent for $Ge_3Sb_2Te_6$ (x = 3/4), gradually weakens on increasing the GeTe-content and eventually fades out in the vicinity of $Ge_8Sb_2Te_{11}$ (x = 8/9). The measurements performed on films step-annealed at 250/275 °C reveal that the electrical properties display the same changes on increasing the GeTe content at fixed annealing temperature as on increasing the annealing temperature of $Ge_1Sb_2Te_4$ (or any other $Ge_1Sb_2Te_4$-like system between $Ge_1Sb_4Te_7$ and $Ge_3Sb_2Te_6$—see Table 1). This similarity strongly suggests that the very same physical mechanism, i.e., disorder-induced electron localization, induces the

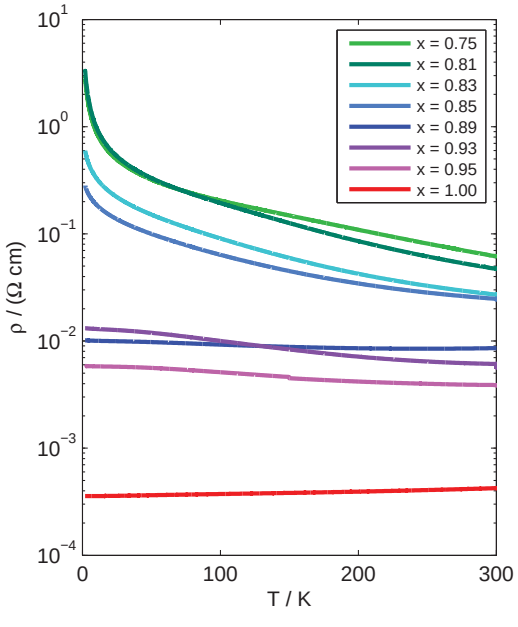

Figure 6. The resistivity as a function of measurement temperature down to 2 K. The color code refers to the stoichiometry x. On increasing the GeTe content (larger values of x), the temperature coefficient evolves from non-metallic behavior ($d\rho/dT < 0$) to metallic behavior ($d\rho/dT > 0$). See Figure 7 for low temperature extrapolations.

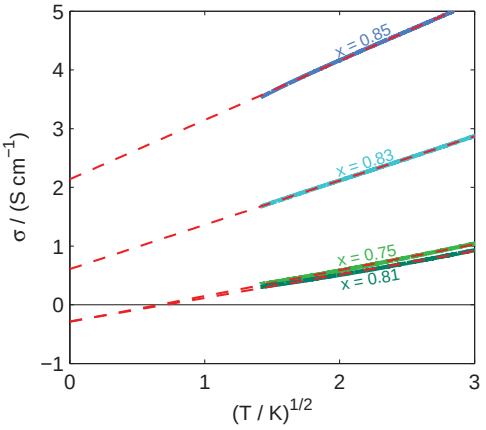

Figure 7. The low-temperature extrapolation according to Equation (4) suggests that the $x \leq 0.81$ films are insulators ($\sigma_0 < 0$), whereas the $x \geq 0.83$ films are metals ($\sigma_0 > 0$).

metal–insulator transition in both cases (T_a variation and x variation). These observations demonstrate that, in addition to the annealing temperature T_a, the GeTe content x can be used as an alternative control parameter for the metal–insulator transition in the $(GeTe)_x$-$(Sb_2Te_3)_{1-x}$ system.

It is noteworthy that the structure parameters change smoothly on increasing the GeTe content of the crystalline alloys between $Ge_3Sb_2Te_6$ and GeTe and that there is no abrupt structural transition. Hence, the stoichiometry sweep between $Ge_3Sb_2Te_6$ and GeTe produces the same evolution of the electrical properties as the annealing-temperature sweep in $Ge_1Sb_2Te_4$ but without any abrupt structural transition. This observation corroborates the statement that the gradual increase in conductivity and the metal–insulator transition in $Ge_1Sb_2Te_4$ cannot be explained in terms of a coexistence of an insulating cubic and a metallic hexagonal crystallographic phase.

The electron localization results from the disorder on the cation sublattice, where according to Zhang et al.[11] vacancy clustering is crucial. The following equation gives the average vacancy concentration on the cation sublattice in the $(GeTe)_x$-$(Sb_2Te_3)_{1-x}$ system

$$n_{vac} = \frac{1-x}{3-2x} \tag{5}$$

As n_{vac} decreases on moving from $Ge_3Sb_2Te_6$ (n_{vac} = 1/6) to GeTe (n_{vac} = 0), the vacancy clusters gradually dissolve and, as a consequence, the localized states disappear. Hence, the ansatz of disorder-induced localization in the $(GeTe)_x$-$(Sb_2Te_3)_{1-x}$ system, which was originally proposed for the annealing series on $Ge_1Sb_2Te_4$, can readily predict the behavior we observed on varying the stoichiometry between $Ge_3Sb_2Te_6$ and GeTe. In this sense, the findings presented in this article underline the explanatory power of this approach.

Supporting Information

Supporting Information is available from the Wiley Online Library or from the author.

Acknowledgements

The authors gratefully acknowledge the support by the Deutsche Forschungsgemeinschaft (SFB 917). Moreover, the research leading to these results has received funding from the European Union Seventh Framework Programme (FP7/2007-2013) under grant agreement no. 340698.

Received: March 3, 2015
Revised: April 20, 2015
Published online: May 21, 2015

[1] N. Yamada, E. Ohno, K. Nishiuchi, N. Akahira, M. Takao, *J. Appl. Phys.* **1991**, *69*, 2849.
[2] M. Wuttig, N. Yamada, *Nat. Mater.* **2007**, *6*, 824.
[3] S. Raoux, *Annu. Rev. Mater. Res.* **2009**, *39*, 25.
[4] T. Zhang, Z. Song, B. Liu, G. Feng, S. Feng, B. Chen, *Thin Solid Films* **2007**, *516*, 42.
[5] E. Prokhorov, G. Trapaga, J. Gonzalez-Hernandez, *J. Appl. Phys.* **2008**, *104*, 103712.
[6] T. Siegrist, P. Jost, H. Volker, M. Woda, P. Merkelbach, C. Schlockermann, M. Wuttig, *Nat. Mater.* **2011**, *10*, 202.
[7] B.-S. Lee, J. R. Abelson, S. G. Bishop, D.-H. Kang, B.-k. Cheong, K.-B. Kim, *J. Appl. Phys.* **2005**, *97*, 093509.
[8] H. Volker, P. Jost, M. Wuttig, *Adv. Funct. Mater.* **2015**, DOI: 10.1002.adfm.201500830.
[9] T. Siegrist, P. Merkelbach, M. Wuttig, *Annual Reviews of Condensed Matter Physics*, Palo Alto, CA **2012**, pp. 215–237.
[10] K. S. Siegert, F. R. L. Lange, E. R. Sittner, H. Volker, C. Schlockermann, T. Siegrist, M. Wuttig, *Rep. Prog. Phys.* **2015**, *78*, 013001.
[11] W. Zhang, A. Thiess, P. Zalden, R. Zeller, P. H. Dederichs, J.-Y. Raty, M. Wuttig, S. Bluegel, R. Mazzarello, *Nat. Mater.* **2012**, *11*, 952.
[12] N. P. Breznay, H. Volker, A. Palevski, R. Mazzarello, A. Kapitulnik, M. Wuttig, *Phys. Rev. B* **2012**, *86*, 205302.
[13] P. Nukala, R. Agarwal, X. Qian, M. H. Jang, S. Dhara, K. Kumar, A. T. C. Johnson, J. Li, R. Agarwal, *Nano Lett.* **2014**, *14*, 2201.
[14] T. Matsunaga, H. Morita, R. Kojima, N. Yamada, K. Kifune, Y. Kubota, Y. Tabata, J. J. Kim, M. Kobata, E. Ikenaga, K. Kobayashi, *J. Appl. Phys.* **2008**, *103*, 093511.
[15] J. Goldak, C. S. Barrett, D. Innes, W. Youdelis, *J. Chem. Phys.* **1966**, *44*, 3323.
[16] E.-R. Sittner, K. S. Siegert, P. Jost, C. Schlockermann, F. R. L. Lange, M. Wuttig, *Phys. Status Solidi A* **2013**, *210*, 147.
[17] K. Shportko, S. Kremers, M. Woda, D. Lencer, J. Robertson, M. Wuttig, *Nat. Mater.* **2008**, *7*, 653.
[18] G. Jellison, F. Modine, *Appl. Phys. Lett.* **1966**, *69*, 371.
[19] M. Fox, *Optical Properties of Solids*, Oxford Master Series in Condensed Matter Physics, Oxford University Press, Oxford **2001**.
[20] W. Theiss Hard- and Software, http://www.wtheiss.com (accessed: April **2015**).
[21] L. R. Doolittle, *Nucl. Instrum. Methods Phys. Res., Sect. B* **1985**, *9*, 344.
[22] I. Friedrich, V. Weidenhof, W. Njoroge, P. Franz, M. Wuttig, *J. Appl. Phys.* **2000**, *87*, 4130.
[23] W. Njoroge, H. Woltgens, M. Wuttig, *J. Vac. Sci. Technol. A* **2002**, *20*, 230.
[24] W. K. Njoroge, H. Dieker, M. Wuttig, *J. Appl. Phys.* **2004**, *96*, 2624.
[25] M. Wuttig, D. Luesebrink, D. Wamwangi, W. Welnic, M. Gillessen, R. Dronskowski, *Nat. Mater.* **2007**, *6*, 122.
[26] P. Konstantinov, L. Shelimova, E. Avilov, M. Kretova, V. Zemskov, *Inorg. Mater.* **2001**, *37*, 662.
[27] T. Kato, K. Tanaka, *Jpn. J. Appl. Phys.* **2005**, *44*, 7340.
[28] S. K. Bahl, K. L. Chopra, *J. Appl. Phys.* **1970**, *41*, 2196.
[29] A. F. Ioffe, A. R. Regel, in *Progress in Semiconductors*, Vol. *4* (Ed: A. F. Gibson), Heywood, London, UK **1960**, pp. 237–291.
[30] O. Gunnarsson, M. Calandra, J. Han, *Rev. Mod. Phys.* **2003**, *75*, 1085.
[31] V. F. Gantmakher, *Electrons and Disorder in Solids*, Clarendon Press, Oxford, UK **2005**.
[32] G. A. Thomas, M. Paalanen, T. F. Rosenbaum, *Phys. Rev. B* **1983**, *27*, 3897.
[33] B. L. Altshuler, A. G. Aronov, P. A. Lee, *Phys. Rev. Lett.* **1980**, *44*, 1288.
[34] P. A. Lee, T. V. Ramakrishnan, *Rev. Mod. Phys.* **1985**, *57*, 287.
[35] M. Woda, *Ph.D. Thesis*, Section 5.2, RWTH Aachen University, **2010**.